# *Col11a2 Deletion Reveals the Molecular Basis for Tectorial Membrane Mechanical Anisotropy*



**Citation:** Masaki, Kinuko, Jianwen Wendy Gu, Roozbeh Ghaffari, Gary Chan, Richard J.H. Smith, Dennis M. Freeman, and A.J. Aranyosi. "Col11a2 Deletion Reveals the Molecular Basis for Tectorial Membrane Mechanical Anisotropy." Biophysical Journal 96, no. 11 (June 2009): 4717–4724. © 2009 Biophysical Society

**As Published:** http://dx.doi.org/10.1016/j.bpj.2009.02.056

**Publisher:** Elsevier

**Persistent URL:** http://hdl.handle.net/1721.1/96782

**Version:** Final published version: final published article, as it appeared in a journal, conference proceedings, or other formally published context

# *Col11a2* Deletion Reveals the Molecular Basis for Tectorial Membrane Mechanical Anisotropy

Kinuko Masaki,[†‡] Jianwen Wendy Gu,[†‡] Roozbeh Ghaffari,[†‡] Gary Chan,[§] Richard J. H. Smith,[¶] Dennis M. Freeman,[†‡§] and A. J. Aranyosi[†*]

[†]Harvard-MIT Division of Health Sciences and Technology and Research Laboratory of Electronics, [§]Department of Electrical Engineering and Computer Science, Massachusetts Institute of Technology, Cambridge, Massachusetts; [‡]Eaton-Peabody Laboratory of Auditory Physiology, Massachusetts Eye and Ear Infirmary, Boston, Massachusetts; and [¶]Department of Otolaryngology—Head and Neck Surgery, University of Iowa, Iowa City, Iowa

ABSTRACT The tectorial membrane (TM) has a significantly larger stiffness in the radial direction than other directions, a prominent mechanical anisotropy that is believed to be critical for the proper functioning of the cochlea. To determine the molecular basis of this anisotropy, we measured material properties of TMs from mice with a targeted deletion of *Col11a2*, which encodes for collagen XI. In light micrographs, the density of TM radial collagen fibers was lower in *Col11a2* –/– mice than wild-types. Tone-evoked distortion product otoacoustic emission and auditory brainstem response measurements in *Col11a2* –/– mice were reduced by 30–50 dB independent of frequency as compared with wild-types, showing that the sensitivity loss is cochlear in origin. Stress-strain measurements made using osmotic pressure revealed no significant dependence of TM bulk compressibility on the presence of collagen XI. Charge measurements made by placing the TM as an electrical conduit between two baths revealed no change in the density of charge affixed to the TM matrix in *Col11a2* –/– mice. Measurements of mechanical shear impedance revealed a 5.5 ± 0.8 dB decrease in radial shear impedance and a 3.3 ± 0.3 dB decrease in longitudinal shear impedance resulting from the *Col11a2* deletion. The ratio of radial to longitudinal shear impedance fell from 1.8 ± 0.7 for TMs from wild-type mice to 1.0 ± 0.1 for those from *Col11a2* –/– mice. These results show that the organization of collagen into radial fibrils is responsible for the mechanical anisotropy of the TM. This anisotropy can be attributed to increased mechanical coupling provided by the collagen fibrils. Mechanisms by which changes in TM material properties may contribute to the threshold elevation in *Col11a2* –/– mice are discussed.

## INTRODUCTION

The tectorial membrane (TM) is an acellular, gel-like tissue that performs at least two essential roles in the cochlea. The TM deflects the mechanosensory bundles of outer hair cells (OHCs), allowing OHCs to increase the sensitivity and frequency selectivity of cochlear motions (1). Moreover, it transmits these motions to the bundles of inner hair cells that send auditory information to the brain (2). The contribution of the TM to cochlear mechanics has been attributed to the presence of a frequency-dependent local radial motion (3–7) and the propagation of traveling waves along the TM (8). To perform these tasks, the TM must be stiff in the radial direction, but it must also be compliant in the longitudinal direction to allow different cochlear regions to be sensitive to different frequencies. It has been shown that the shear impedance of the TM is roughly twice as large in the radial direction as in other directions (9–13). A model suggests that this anisotropy is due to the presence of radially oriented collagen fibrils (13), a feature that is unique to the mammalian TM among hair cell tectorial structures (14). However, the extent to which these fibers contribute to TM mechanical properties has not been determined experimentally.

The radial collagen fibrils of the TM consist primarily of collagen type II covalently linked to lesser amounts of collagen types IX and XI, and possibly V (14–17). A mouse model of genetic hearing loss allows us to investigate how these radial collagen fibrils affect TM stiffness and cochlear sensitivity. Humans with genetic deafness linked to the DFNA13 locus on chromosome 6p have prelingual, nonprogressive midfrequency hearing loss associated with a disruption of the radial fibrillar structure of the TM (18,19). The gene associated with this locus, *COL11A2*, encodes for subunit $\alpha$-2 of collagen type XI, a quantitatively minor fibrillar component of the TM (17). Transgenic mice lacking *Col11a2* have 40–50 dB threshold elevation as measured at the brainstem (19). In *Col11a2* –/– mice, the radial fibrillar structure of the TM is disorganized and the collagen fibrils are more widely spaced than in wild-type mice. Here we report measurements of bulk compressibility, fixed charge concentration, and shear impedance of TMs from wild-type and *Col11a2* –/– mice (hereafter referred to as wild-type and *Col11a2* –/– TMs). These measurements allow us to examine the contribution of radial collagen fibrils to TM mechanical properties, and suggest that changes in TM radial stiffness may underlie DFNA13-related hearing loss.

*Submitted November 25, 2008, and accepted for publication February 13, 2009.*

*Correspondence: aja@mit.edu

Kinuko Masaki's present address is Stanford University, Department of Otolaryngology, Head & Neck Surgery, 801 Welch Rd., Stanford, CA 94305.

Gary Chan's present address is L-1 Identity Solutions, 296 Concord Rd., Billerica, MA 01821.

Editor: Richard E. Waugh.



0006-3495/09/06/4717/8 $2.00

doi: 10.1016/j.bpj.2009.02.056

# METHODS

## Methods for measuring DPOAEs and ABRs

All distortion product otoacoustic emission (DPOAE) and auditory brainstem response (ABR) measurements were conducted at the Massachusetts Eye and Ear Infirmary. The methods used to measure DPOAEs and ABRs have been described in detail previously (20). For both of these measurements, mice were anesthetized with xylazine (20 mg/kg) and ketamine (100 mg/kg). All electrophysiological experiments were conducted in a soundproof anechoic chamber maintained at ~32°C.

## DPOAE measurements

DPOAEs at $2f_1$-$f_2$ were recorded with a custom acoustic assembly consisting of two 6.3-mm diameter condenser microphones used to generate the two primary tones and a Knowles miniature microphone (EK3103; Knowles Electronics, Franklin Park, IL) used to record sound pressure in the ear canal. Stimuli were generated digitally (A0-6; National Instruments, Austin, TX). The tone pip frequencies for the second primary frequency, $f_2$, were 5.65, 8.0, 11.3, 16.0, 22.65, 32.0, and 45.25 kHz, and the $f_2/f_1$ frequency ratio was 1.2. The level of the $f_1$ tone was increased in 5 dB steps from 10 dB below threshold to 80 dB SPL. The $f_2$ sound level was 10 dB below the $f_1$ sound level. The sound pressure recorded by the microphone was amplified and digitized, and the Fourier transform computed. The level of the $2f_1$–$f_2$ DPOAE was determined from the average of five Fourier transforms of separate measurements. DPOAE threshold was defined as the $f_2$ level required for the DPOAE level to be 1.5 dB SPL.

## ABR measurements

ABR measurements were made using the same acoustic assembly used for the DPOAEs. ABRs were recorded from electrodes inserted into the vertex, pinna, and tail. The electrode at the tail served as the grounding electrode. ABR potentials were evoked with 5 ms tone pips at the DPOAE $f_2$ frequencies. The tone level was increased in 5 dB steps from 10 dB below threshold up to 80 dB SPL. At each SPL, 1024 responses with alternating stimulus polarity were amplified by 80 dB, band-pass filtered from 0.1–2 kHz, and averaged using a LabVIEW data-acquisition system (National Instruments). Waveforms with peak-to-peak amplitudes exceeding 15 $\mu$V were typically caused by motion of the animal and were discarded. ABR threshold was determined by visual inspection.

## Preparation of the isolated TM

*Col11a2* transgenic and wild-type mice 6–10 weeks old were asphyxiated with $CO_2$ and then decapitated. The pinnae and surrounding tissues were removed and the temporal bone was isolated. While observing through a dissecting microscope, the temporal bone was chipped away with a scalpel to isolate the cochlea. The cochlea was placed in an artificial endolymph (AE) solution containing (in mmol/L): 174 KCl, 2 NaCl, 0.02 $CaCl_2$, and 5 HEPES, with pH adjusted to 7.3. The cochlea was widely opened to allow access to the organ of Corti. The TM was isolated from the rest of the organ by probing the organ with an eyelash. Individual pieces of TM, primarily from the apical and middle turns, were located and transferred via pipette to a glass slide. The slide was prepared with 0.3 $\mu$L of Cell-Tak adhesive (BD Biosciences, Bedford, MA) to immobilize the TM on the slide surface. This immobilization served three purposes:

1. It kept the TM from being carried out with the effluent as various fluids were perfused.
2. It allowed microfabricated probes to exert shearing forces rather than displace the bulk of the TM.
3. It allowed TM volume to be calculated by tracking the positions of beads on the TM and the surrounding glass slide.

## Measuring stress-strain relation

The methods used to measure the stress-strain relation of the TM have been published previously (21). Briefly, the TMs from *Col11a2* –/– and wild-type mice were placed on a glass slide. The surface of the TM was decorated with TransFluoSphere carboxylate-modified fluorescent microspheres (i.e., beads) to improve visualization of the TM surface. The TM was immersed in AE containing various concentrations of polyethylene glycol (PEG) with a molecular mass of 511 kDa. The applied osmotic pressure for each solution ranged from 0–10 kPa, and was computed from the concentration and molecular mass of PEG as described previously (21). Sets of 100 images of the TM taken at focal depths spaced 1-$\mu$m apart were recorded once per minute after the specimen was immersed in a given solution for at least 1 h. One hour was found to be sufficient time for the TM to stabilize (22). The positions of beads on the surface were tracked from these volumetric images to determine changes in TM height in solutions of different compositions. The positional accuracy of these measurements was ~0.1 mm. The z component of the strain, $\epsilon_z$, is given by

$$\epsilon_z = 1 - v_z, \tag{1}$$

where $v_z$ is the ratio of bead height in the presence of PEG to that in its absence. The relation between osmotic pressure $\sigma_{osm}$ and $\varepsilon_z$ was characterized by a power law, $\varepsilon_z = A\sigma_{osm}^b$, where $A$ and $b$ are constants determined by a least-squares fit. The longitudinal modulus, a basic material property of the TM, is defined by the derivative $\partial\sigma_{osm}/\partial\varepsilon_z$ of this relation (21).

## Measuring fixed charge concentration

Fixed charge groups within the TM attract mobile counterions, and thus establish an electrical potential between the TM and the bath according to the Donnan relation (23). This potential is given by

$$V = \frac{RT}{F}\ln\left(\sqrt{\left(\frac{c_f}{C_\Sigma}\right)^2 + 1} - \frac{c_f}{C_\Sigma}\right), \tag{2}$$

where $V$ is the potential of the TM, $F$ is Faraday's constant, $C_\Sigma$ is the sum of concentrations of all ions in the bath, $R$ is the molar gas constant, $T$ is absolute temperature, and $c_f$ is the concentration of fixed charges within the TM. This potential is formed at the surface of the TM, and is valid for length scales large compared with the Debye length. Since the TM lacks an insulating membrane, the electrical impedance between the inside and outside of the TM is small. Consequently, the Donnan potential is difficult to measure using microelectrodes, which have a relatively high impedance. When the TM forms an electrical conduit between two baths, however, a Donnan potential is established between the TM and each bath. The potential difference $V_D$ between baths can be measured with low-impedance electrodes, and is related to the fixed charge concentration $c_f$ of the TM by

$$V_D = \frac{RT}{F}\ln\left(\frac{\sqrt{\left(\frac{c_f}{C_R}\right)^2 + 1} - \frac{c_f}{C_R}}{\sqrt{\left(\frac{c_f}{C_T}\right)^2 + 1} - \frac{c_f}{C_T}}\right), \tag{3}$$

where $C_R$ and $C_T$ are $C_\Sigma$ for the reference and test baths, respectively. When $C_R$ and $C_T$ are equal, or are large compared with $c_f$, $V_D \approx 0$. As $C_T$ is lowered, however, $V_D$ becomes increasingly negative. By measuring $V_D$ as a function of $C_T$ while keeping $C_R$ constant, we can determine $c_f$ from the fit of Eq. 3 to the measurements. Note that $V_D$ depends only on the concentrations of fixed and mobile charges near the boundaries between the TM and the baths. The spatial dependence of mobile ion concentration within the main body of the TM determines the local spatial gradient of potential but does not affect $V_D$.

To measure $V_D$, we developed a planar-clamp technique (24,25). The TM was placed directly over a 15-$\mu$m radius microaperture, which separated two

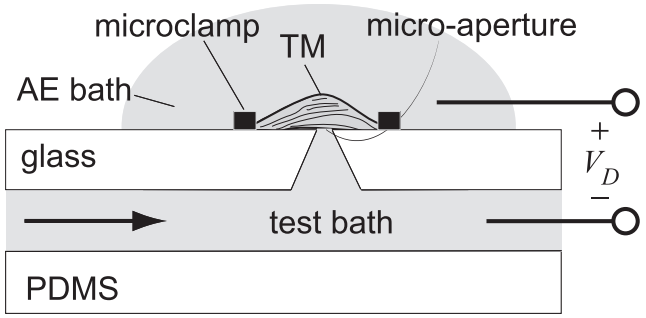


FIGURE 1 Planar-clamp chamber for measuring TM electrical properties. The TM was placed over a 15-$\mu$m radius aperture that separates two baths. The aperture was made in a coverslip, while the lower bath was cast in poly(dimethylsiloxane). The top bath contained AE with a KCl concentration of 174 mM. The test bath contained modified AE with KCl concentrations of 21–174 mM. The electrical potential between baths was measured with low-impedance electrodes and used to determine the concentration of charge in the TM according to Eq. 3.

bath solutions of differing ionic strengths (Fig. 1). The microaperture was laser-drilled (Lenox Laser, Glen Arm, MD) from a 200–300 $\mu$m thick coverslip. The small size of the aperture guaranteed that the sole electrical pathway connecting the baths passed through the TM. This coverslip was glued to a piece of poly(dimethylsiloxane), which had been cast to contain a small fluid channel for perfusing a test bath. The resulting device supported two fluid baths, one on either side of the microaperture. The upper reference bath contained AE, whereas the lower test bath contained variants of AE with a range of KCl concentrations: 21, 32, 43, 87, and 174 mM. The bulk of the TM was in contact with the reference bath to minimize TM volume changes in response to changes in the test bath.

The electrical potential between the baths was measured with Ag/AgCl microelectrodes (A-M Systems, Sequim, WA) immersed in large-tip micropipettes containing 3 M KCl and agarose. These electrodes were coupled through an amplifier (DAM60-G Differential Amplifier, World Precision Instruments, Miami, FL) to a multimeter (TX3 True RMS Multimeter, Tektronix, Beaverton, OR) connected to a computer. DC and AC potentials were read from the multimeter by the computer every 2–3 s. The presence of AC potentials was taken as evidence of electrical noise. Recordings were rejected if the magnitude of the AC potential exceeded the DC potential. Each test bath was perfused for 10–30 min at a time, and each bath was perfused at least twice over the course of an experiment.

In addition to the Donnan potential, a liquid junction potential (LJP) can be established between the two baths. This LJP occurs because the ions diffusing across the boundary may have differing mobilities; when one ion diffuses more quickly, a potential is established to maintain an electrodiffusive equilibrium. In these experiments, this LJP was expected to be small, since $K^+$ and $Cl^-$ have similar mobilities. Additional factors, such as junction potentials between the electrodes and the bath, can also contribute to the measured potential. The contribution of these various factors to the potential was determined by periodically lifting the TM from the hole and measuring the resulting potential. This potential was subtracted from the potential measured with the TM in place to determine $V_D$.

## Measuring shear impedance

Shearing forces were applied in both the radial and longitudinal direction by means of a microfabricated probe, as described in a previous publication (12). The probe consisted of a base that was driven by a piezoactuator, a 30 × 30 $\mu$m shearing plate that contacted the TM, and flexible arms that connected the base to the plate. A micromanipulator was used to position the microfabricated probe on the TM surface. Displacements of ~0.5–1 $\mu$m were applied by means of the piezoactuator at audio frequencies of 10–9000 Hz. Stroboscopic illumination was used to collect images of the TM and the probe at eight evenly spaced phases of the stimulus. Optical flow algorithms were used to measure displacements of both the probe and the TM relative to the base (26,27).

The impedance of the TM was calculated from the displacement data. In the frequency domain, the impedance $Z_{TM}(\omega)$ is related to the applied force $\Phi(\omega)$ and the measured displacements of the probe base $X_b(\omega)$ and shearing plate $X_p(\omega)$ by

$$Z_{TM}(\omega) = \frac{k_{TM}}{j\omega} + b_{TM} = \frac{F(\omega)}{V(\omega)} = k_{mp}\frac{X_b(\omega) - X_p(\omega)}{j\omega X_p(\omega)}, \quad (4)$$

where $k_{TM}$ and $b_{TM}$ are the stiffness and damping of the TM, respectively; $V(\omega) = j\omega X_p(\omega)$ is the velocity of the TM and shearing plate; and $k_{mp}$ is the stiffness of the microfabricated probe. As in the previous study, the frequency dependence of TM shear impedance showed no significant contribution from TM mass, so the mass term was left out of Eq. 4. As shown previously, the presence of fluid surrounding the TM and probe caused the magnitude of longitudinal shear impedance to increase by up to 50% and the phase to become less negative at frequencies above 2 kHz (12). The presence of fluid did not affect shear impedance measurements at lower frequencies.

## Genotyping of mice and animal care

Genotyping was done by MIT's Department of Comparative Medicine following published methods (28). The care and use of animals reported in this study were approved by the Massachusetts Institute of Technology Committee on Animal Care.

# RESULTS

## *Col11a2* –/– TMs have a lower density of radial collagen fibrils

Fig. 2 shows light micrographs of TMs from wild-type and *Col11a2* –/– mice. Several prominent structures are visible in both images. Hensen's stripe, which is located adjacent to the hair bundles of inner hair cells, appeared unaffected by the *Col11a2* disruption. The radial fibrillar structure of the TM was still visible in *Col11a2* –/– TMs. However, the density of radial collagen fibers decreased. In images of wild-type TMs, the brightness of the fibers cycled between light and dark roughly every 2 $\mu$m. In *Col11a2* –/– TMs, this modulation spanned a distance of ~4 $\mu$m. Thus, the deletion appeared to reduce the density of radial fibers.

## ABR and DPOAE measurements

Previous ABR measurements with click-evoked stimuli showed that *Col11a2* –/– mice have elevated auditory thresholds, but did not localize the origin of the threshold elevation (19). To identify the portion of the auditory system responsible, we compared threshold elevations in *Col11a2* –/– mice using two techniques that probe different aspects of the auditory pathway. ABRs measure the response of the auditory system up to the brainstem, whereas DPOAEs measure properties of the middle ear and cochlea. Fig. 3 shows the DPOAE threshold as a function of frequency for *Col11a2* –/– mice and wild-types. For wild-type mice, the DPOAE threshold was lowest at 16 kHz. The thresholds

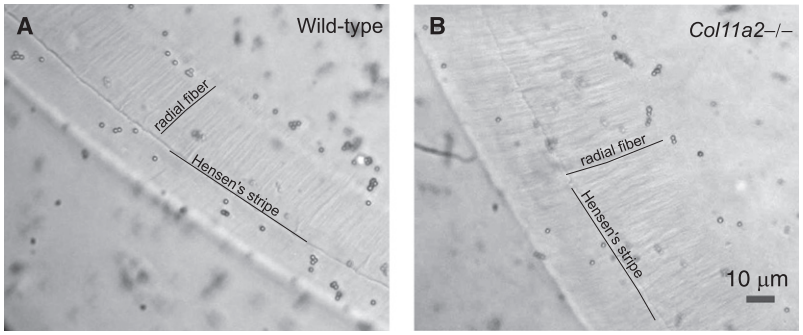


FIGURE 2 Light micrographs of TMs from (*A*) wild-type and (*B*) *Col11a2* –/– mice taken using bright-field imaging. The TM extends from the upper left to lower right of each image. Radial fibrils and Hensen's stripe are visible in both images. However, the density of radial fibrils is lower in the *Col11a2* –/– TM. The circles scattered throughout the image are microbeads that were used to track TM volume changes in response to osmotic pressure.

increased for higher and lower frequencies. Between 10 and 25 kHz, the DPOAE thresholds of *Col11a2* –/– mice were 30–40 dB higher than those of wild-types. In this range of frequencies, the threshold elevation showed no significant dependence on frequency. At lower and higher frequencies, the threshold elevation was masked by the presence of nonlinearities in the measurement system.

Measured ABR thresholds as a function of frequency are shown in Fig. 4. Unlike the DPOAE measurements, the ABR thresholds were relatively flat as a function of frequency. The ABR thresholds for *Col11a2* –/– mice were 30–50 dB higher than those of wild-types over the entire frequency range measured. No significant dependence of ABR threshold elevation on frequency was seen. Moreover, between 10 and 25 kHz, for which DPOAE measurements were not masked by system nonlinearities, the threshold elevations seen in DPOAE and ABR measurements were similar in magnitude.

## Stress-strain relation

To determine whether the *Col11a2* deletion affected the longitudinal modulus of the TM, the transverse component of TM strain was measured in response to applied osmotic stress. Fig. 5 shows the stress-strain relation of TM segments from wild-type and *Col11a2* –/– mice. Strains for *Col11a2* –/– TMs averaged 75–80% of those for wild-type TMs for stresses $\geq 1$ kPa, but the ranges for the two populations overlapped. For smaller stresses, no difference in strain between wild-type and *Col11a2* –/– TMs was seen.

The relation between stress and strain was nonlinear, and roughly followed a power-law relation. For wild-type TMs, the best-fit power-law relation was $\varepsilon_z = (0.27 \pm 0.06)\sigma_{osm}^{(0.32 \pm 0.1)}$ ($n = 7$ TMs), with $\sigma_{osm}$ in kPa. For *Col11a2* –/– TMs, this relation was $\varepsilon_z = (0.23 \pm 0.06)\sigma_{osm}^{(0.24 \pm 0.1)}$ ($n = 6$ TMs). The differences between these fits were not statistically significant.

## TM fixed charge concentration

The presence of charge in the TM has been attributed to negatively-charged glycosaminoglycan groups attached to the striated-sheet matrix (14,29). Although this matrix is distinct from the collagen fibers (30), any potential interactions of the two could affect the charge density of the TM in *Col11a2* –/– mice. To test this possibility, the concentration of fixed charge within the TM was measured electrically. The voltage between two dissimilar baths connected by

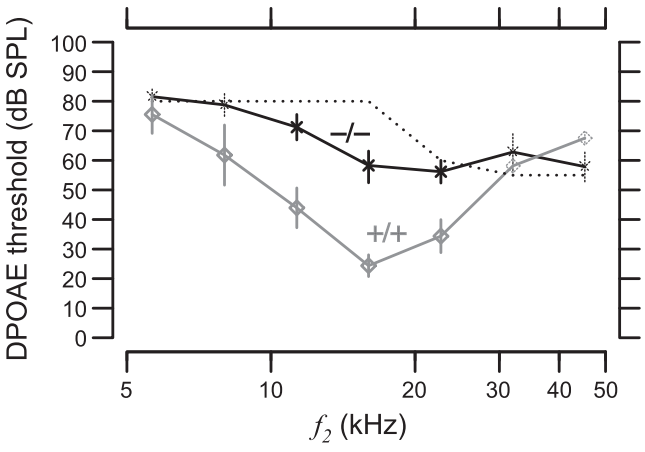


FIGURE 3 DPOAE threshold of *Col11a2* –/– mice ($n = 36$) compared with wild-types ($n = 5$). Plot symbols represent the median threshold and the lengths of the vertical lines show the interquartile range. The dotted line represents the sound pressure level above which nonlinearities of the measurement system obscured DPOAE measurements. Symbols drawn with thinner dashed lines had median values that were at or above the threshold for nonlinearity.

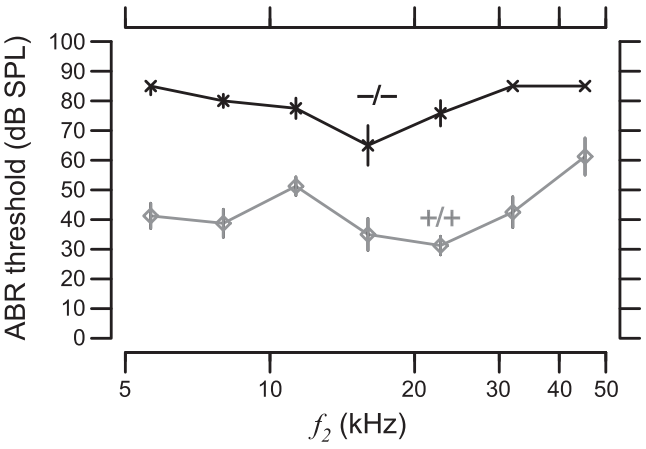


FIGURE 4 ABR threshold of *Col11a2* –/– mice ($n = 36$) compared with wild-types ($n = 5$). Plot symbols represent the median threshold and the lengths of the vertical lines show the interquartile range.

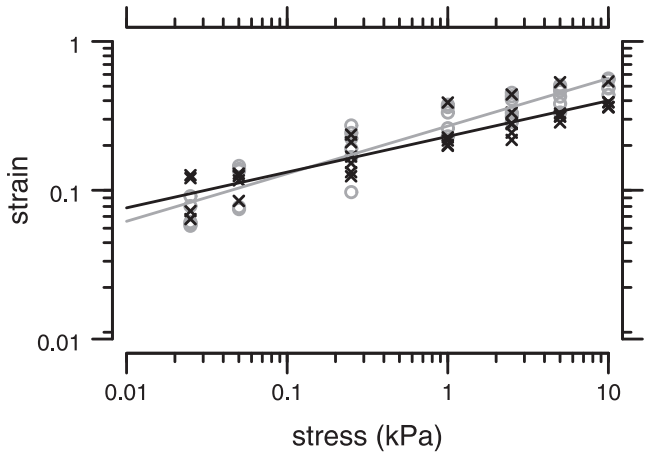


FIGURE 5 TM stress-strain relation for *Col11a2* –/– ($n = 7$) and wild-type ($n = 7$) TM segments. The plot symbols represent the median value for each measurement on TM segments from wild-type (*shaded circles*) and *Col11a2* –/– (*solid crosses*) mice. The curves are least-squares fits of a power-law relation to the measurements.

the TM depends on the ionic composition of the baths and the concentration of fixed charge within the TM, as described by Eq. 3. Fig. 6 summarizes measurements of the voltage across the TM as a function of the concentration of KCl in the test bath for TM segments from wild-type and *Col11a2* –/– mice. For both wild-type and *Col11a2* –/– TM segments, the measured potential difference became more negative for smaller test bath KCl concentrations. No significant difference in potentials was seen between wild-type and *Col11a2* –/– mice over the range of test bath KCl concentrations measured.

The fixed charge concentrations $c_f$ of TMs from *Col11a2* –/– and wild-type mice were determined by fitting Eq. 3 to the measured voltages in a least-squares sense. The voltages predicted from these fits fell within the interquartile

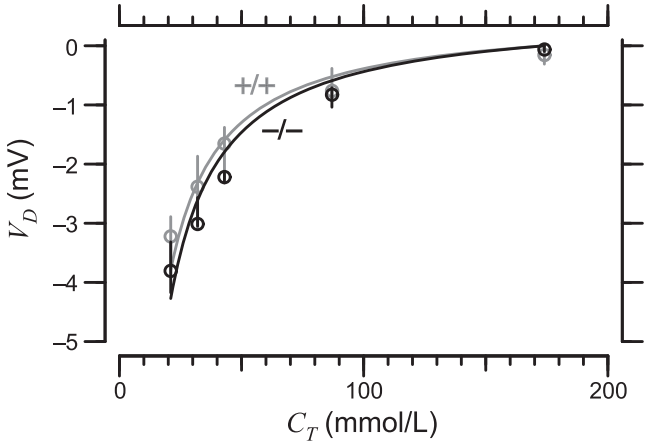


FIGURE 6 Potential difference $V_D$ between two baths as a function of KCl bath concentration $C_T$ for TM segments from wild-type (*shaded*, $n = 5$) and *Col11a2* –/– (*solid*, $n = 3$) mice. Circles are the median values and vertical lines show the interquartile ranges of the measurements. The solid line is the least-squares fit of the medians to the Donnan relation.

range of the measured voltage for nearly all bath concentrations. The best fit $c_f$ values for wild-type and *Col11a2* –/– TMs were $-6.4 \pm 1.4$ ($n = 5$) and $-9.8 \pm 3.7$ ($n = 3$) mmol/L, respectively. These values were not significantly different.

### TM shear impedance

Because the collagen fibers that were disrupted in *Col11a2* –/– mice are oriented primarily in the radial direction, the *Col11a2* –/– disruption was expected to preferentially affect the radial shear impedance of the TM. To evaluate this prediction, measurements of shear impedance in both the radial and longitudinal directions were made at multiple frequencies using a microfabricated probe. Fig. 7 summarizes the magnitude and phase of shear impedance for TM segments from wild-type and *Col11a2* –/– mice. The magnitudes of the shear impedance for the TMs from *Col11a2* –/– mice ($n = 3$) were $5.5 \pm 0.8$ dB lower than wild-types ($n = 5$) in the radial direction. In the longitudinal direction, shear impedance magnitude was $3.3 \pm 0.3$ dB lower for *Col11a2* –/– mice than for wild-types. The slopes of shear impedance magnitude versus frequency for wild-type TMs were $16 \pm 0.4$ dB/decade for radial forces and $19 \pm 0.5$ dB/decade for longitudinal forces. For *Col11a2* –/– TMs, these slopes were $16 \pm 1.0$ dB/decade and $19 \pm 0.8$ dB/decade, respectively. The ratio of radial to longitudinal impedance at 10 Hz was $1.0 \pm 0.1$ for *Col11a2* –/– TMs versus $1.8 \pm 0.7$ for wild-type TMs. Thus, the *Col11a2* deletion eliminated the anisotropy of TM shear impedance. The phases of shear impedance for wild-type TMs were $-72 \pm 6°$ for radial forces and $-74 \pm 11°$ for longitudinal forces below 4 kHz. For *Col11a2* –/– TMs, these phases were $-74 \pm 4°$ and $-72 \pm 10°$, respectively. Neither the slopes nor the phases differed significantly between wild-type and *Col11a2* –/– TMs. These results indicate that the deletion reduced the elastic and viscous contributions to impedance in equal proportion. The presence of fluid caused the measured phase of longitudinal shear impedance to increase for frequencies $\geq 4$ kHz. This effect also increased the measured impedance magnitude slightly at these frequencies, but this increase is masked by the logarithmic scale of the plot.

## DISCUSSION

### Threshold elevation in *Col11a2* –/– mice is cochlear in origin

In *Col11a2* –/– mice, both DPOAE and ABR thresholds are elevated by 30–50 dB between 10 and 25 kHz. Since ABR measures neural activity in the brainstem, whereas DPOAE measures mechanical properties of the cochlea and middle ear, these results imply that the threshold elevation in *Col11a2* –/– mice has a mechanical basis. If the loss were due to changes in the middle ear, it would affect both the forward and reverse transmission of sound, causing DPOAE thresholds to increase more than ABR thresholds (31). The similar threshold elevation for ABR and DPOAE

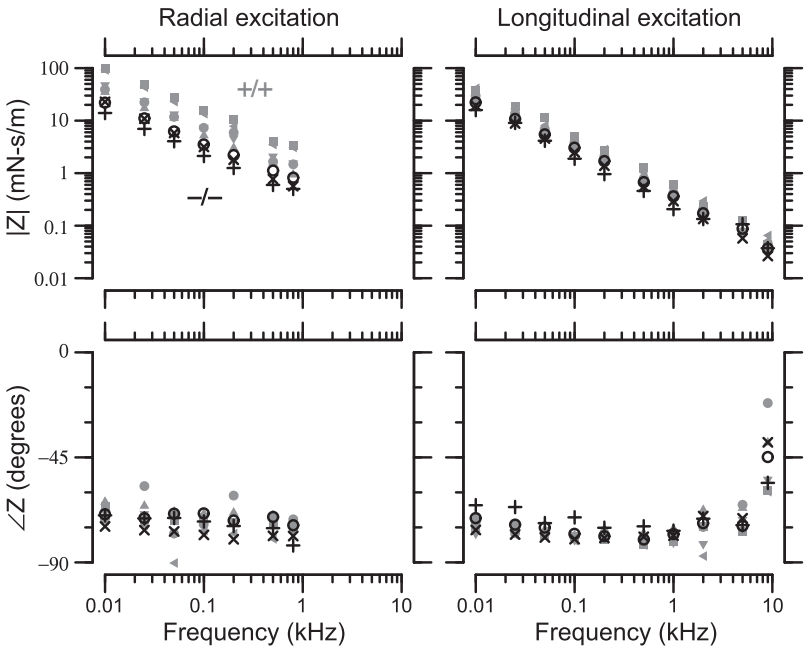


FIGURE 7 Magnitude (*top*) and phase (*bottom*) of shear impedance as a function of frequency for both radial (*left*) and longitudinal (*right*) excitation. The plot symbols represent individual measurements from wild-type ($n = 5$, *shaded symbols*) and *Col11a2* –/– ($n = 3$, *solid symbols*) TMs. Shaded symbols are from Gu et al. (12).

measurements indicates that the *Col11a2* deletion affects sensitivity through mechanical changes within the cochlea. Since the only visible morphological abnormalities within the cochleas of *Col11a2* –/– mice were in the TM (19), it is reasonable to conclude that the threshold elevation in these mice is related to changes within the TM.

## Nonlinear stress-strain relation of the TM

A previous study of the response of the TM to osmotic pressure showed that the stress-strain relation was nonlinear (21,32). The current results support this previous finding, and demonstrate that the stress-strain relation of the TM does not depend significantly on the presence of collagen type XI. The physical basis of this nonlinearity is unknown. One potential source of nonlinearity is the presence of fixed charge within the striated-sheet matrix of the TM (23). The contribution of fixed charge to the longitudinal modulus increases as the TM is compressed, so the charge-related stress is proportional to $1/(1 - \varepsilon_z)$. However, this nonlinearity is significant only for $\varepsilon_z > 0.1$, so it does not explain the nonlinearity at the lowest strains. It is possible that the charge is distributed nonuniformly, so that even the smallest stresses applied here caused local increases in fixed charge concentration. Alternately, the charge-independent mechanical properties of the striated-sheet matrix may contribute nonlinearity to the elastic modulus. Regardless of the physical basis for this nonlinearity, it appears to be unaffected by the lack of collagen XI in *Col11a2* –/– mice.

## TM mechanical anisotropy is due to collagen

Among hair cell organs, the presence of collagen in the overlying gelatinous matrix is unique to the mammalian TM (14,34). A computational model of TM material properties suggests that the radial stiffness of the TM is dominated by these collagen fibrils (13). Moreover, radial variations in TM shear modulus are correlated with the local density of collagen fibrils (35). Fig. 7 shows that the *Col11a2* deletion eliminated the difference between radial and longitudinal shear impedance, demonstrating that the mechanical anisotropy of the TM is due to collagen. However, collagen type XI makes up only a small fraction of the total collagen in the TM. Thus, the effect on TM shear impedance of a targeted disruption in collagen XI is most likely an indirect one.

In cartilage, collagen type XI is thought to be important for maintaining the interfibrillar spacing and fibril diameter of collagen type II (36–38). Therefore, we expect the deletion of collagen type XI to affect the organization and strength of the radial fibers in the TM. This argument is supported by the decrease in fibril density seen in light micrographs in the current study, and by electron micrographs that show loss of organization of the collagen fibrils in *Col11a2*knock-out mice (19). It is further supported by the fact that the longitudinal shear impedance also decreased, but by a lesser amount. Since the fibrils are oriented at an angle relative to the radial direction, any reduction in fibril density would reduce shear impedance in the longitudinal as well as the radial direction.

Perhaps the most surprising finding was that the radial shear impedance decreased by only a factor of two. This finding, and the fact that shear impedance is only twice as large radially as longitudinally in wild-type TMs, suggests that the shear impedance is not dominated by the material properties of the fibrils themselves. As we discuss below, the linking of collagen fibrils by collagen XI appears to increase the extent of the TM over which the applied shear stress is

distributed. Thus, the primary role of TM collagen in response to shearing forces appears to be to provide coupling rather than elasticity.

### *Col11a2* increases coupling within the TM

Although the magnitude of shear impedance measured in *Col11a2* –/– mice decreased as compared with wild-types, the phase was unaffected. This result indicates that the deletion reduced not only the elastic contribution to impedance, but the viscous component as well. Such a finding is somewhat surprising, since collagen is generally believed to provide elastic strength. However, this finding can be explained by the fact that collagen XI is a linking protein that couples individual collagen II fibrils together. As a result, the volume of TM over which the applied shear stress is distributed is larger in the presence of collagen XI than in its absence. Because the impedance of the TM is distributed, the magnitude of shear impedance is determined by the volume of TM over which the force is applied. However, the phase depends on the relative contribution of elasticity and damping to the response, which is determined by the local molecular properties of the tissue. Because these local properties are not affected by the extent of coupling, the *Col11a2* deletion affects only the magnitude of TM shear impedance.

Another intriguing aspect of the shear impedance measurements is that the phase of impedance is independent of frequency. This result shows that the relative contribution of elasticity and damping to shear impedance remains constant over at least two decades of frequency. Similar frequency-independent phases are seen in the elastic modulus of cartilage under tension (39) at $10^{-3}$–$10^{-1}$ Hz, in the shear modulus of cartilage at 20–1000 Hz (40), and in the dynamic modulus of arterial wall (41) at 1–20 Hz. Such frequency-independent phase responses are not consistent with the three simplest models of viscoelasticity: the Maxwell, Voigt, and Kelvin models (42). However, these responses can be predicted by a generalization of the Kelvin model in which the two mechanical relaxation rates are replaced by a continuous relaxation spectrum (42). The range of frequencies over which the impedance phase is roughly constant is determined by the frequency range of the relaxation spectrum. The higher frequency range for shearing as compared with normal forces seen in various tissues presumably reflects the relative resistance to bulk fluid displacement induced by normal forces versus local fluid displacement induced by shear.

### Alteration of TM radial collagen fibers may cause threshold elevation

As mentioned above, the similarity in loss for ABR and DPOAE measurements implies that the threshold elevation in *Col11a2* –/– mice results from a mechanical change inside the cochlea. Because the only obvious morphological change in cochleas of *Col11a2* –/– mice was the disruption of collagen fibrils within the TM (19), it seems reasonable to attribute the threshold elevation to a change in the TM. We cannot attribute the threshold elevation to a simple reduction in radial shear impedance; a parallel study in *Tecta*$^{Y1870C/+}$ mice (K. Masaki, R. Ghaffari, J. W. Gu, G. P. Richardson, D. M. Freeman, and A. J. Aranyosi, unpublished), whose mutation affects the striated-sheet matrix of the TM, found a similar reduction in shear impedance with little change in DPOAE threshold. Because the collagen fibers provide mechanical coupling in the radial direction, a disruption of these fibers could inhibit the radial TM motion that is believed to drive OHC hair bundle deflection (5–7). This loss of radial coupling could also affect the ability of the three rows of OHCs to act in concert by allowing their hair bundles to be deflected independently. In addition, the elimination of TM anisotropy could have a significant impact on the longitudinal propagation of radial shearing waves along the TM (8). Finally, it has been suggested that mechanical anisotropy of the TM is essential for the deflection of OHC hair bundles by the TM (43). In that study the surface of the TM facing OHC bundles was found to be most rather than least compliant in the radial direction; nonetheless, collagen fibrils are likely to be responsible for this anisotropy as well (44). Because of the close proximity of the TM to OHCs, these mechanisms or others not discussed here can have a significant impact on the excitation of OHCs, and therefore on cochlear mechanical function.

We thank Chris Shera, Tony Ricci, and the members of the MIT Micromechanics Group for their insightful comments. Stephane Maison provided invaluable support with ABR and DPOAE measurements.

G.C., A.J.A., and D.M.F. were supported by National Institutes of Health (NIH) grant No. R01-DC00238. J.W.G. and R.G. were supported by an NIH training grant to the Harvard-MIT Speech and Hearing Biosciences and Technology Program. K.M. and R.J.H.S. were supported in part by NIH-NIDCD grant No. R01 DC03544.

## REFERENCES

1. Russell, I. J., P. K. Legan, V. A. Lukashkina, A. N. Lukashkin, R. J. Goodyear, et al. 2007. Sharpened cochlear tuning in a mouse with a genetically modified tectorial membrane. *Nat. Neurosci.* 10: 215–223.
2. Legan, P. K., V. A. Lukashkina, R. J. Goodyear, A. N. Lukashkin, K. Verhoeven, et al. 2005. A deafness mutation isolates a second role for the tectorial membrane in hearing. *Nat. Neurosci.* 8:1035–1042.
3. Zwislocki, J. J. 1979. Tectorial membrane: a possible sharpening effect on the frequency analysis in the cochlea. *Acta Otolaryngol.* 87:267–269.
4. Allen, J. B. 1980. Cochlear micromechanics—a physical model of transduction. *J. Acoust. Soc. Am.* 68:1660–1670.
5. Gummer, A. W., W. Hemmert, and H.-P. Zenner. 1996. Resonant tectorial membrane motion in the inner ear: its crucial role in frequency tuning. *Proc. Natl. Acad. Sci. USA.* 93:8727–8732.
6. Hemmert, W., H. P. Zenner, and A. W. Gummer. 2000. Three-dimensional motion of the organ of Corti. *Biophys. J.* 78:2285–2297.
7. Cai, H., B. Shoelson, and R. S. Chadwick. 2004. Evidence of tectorial membrane radial motion in a propagating mode of a complex cochlear model. *Proc. Natl. Acad. Sci. USA.* 101:6243–6248.
8. Ghaffari, R., A. J. Aranyosi, and D. M. Freeman. 2007. Longitudinally propagating traveling waves of the mammalian tectorial membrane. *Proc. Natl. Acad. Sci. USA.* 104:16510–16515.

9. Abnet, C. C., and D. M. Freeman. 2000. Deformations of the isolated mouse tectorial membrane produced by oscillatory forces. *Hear. Res.* 144:29–46.
10. Freeman, D. M., C. C. Abnet, W. Hemmert, B. S. Tsai, and T. F. Weiss. 2003. Dynamic material properties of the tectorial membrane: a summary. *Hear. Res.* 180:1–10.
11. Richter, C.-P., G. Emadi, G. Getnick, A. Quesnel, and P. Dallos. 2007. Tectorial membrane stiffness gradients. *Biophys. J.* 93:2265–2276.
12. Gu, J. W., W. Hemmert, D. M. Freeman, and A. J. Aranyosi. 2008. Frequency-dependent shear impedance of the tectorial membrane. *Biophys. J.* 95:2529–2538.
13. Gavara, N., and R. Chadwick. 2009. Measurement of anisotropic mechanical properties of the tectorial membrane. *In* Mechanics of Hearing. N. P. Cooper and D. T. Kemp, editors. World Scientific, Singapore. In press.
14. Richardson, G. P., I. J. Russell, V. C. Duance, and A. J. Bailey. 1987. Polypeptide composition of the mammalian tectorial membrane. *Hear. Res.* 25:45–60.
15. Thalmann, I., G. Thallinger, E. C. Crouch, T. H. Comegys, N. Barrett, et al. 1987. Composition and supramolecular organization of the tectorial membrane. *Laryngoscope.* 97:357–367.
16. Slepecky, N. B., J. E. Savage, L. K. Cefaratti, and T. J. Yoo. 1992. Electron-microscopic localization of type II, IX, and V collagen in the organ of Corti of the gerbil. *Cell Tissue Res.* 267:413–418.
17. Thalmann, I. 1993. Collagen of accessory structures of organ of Corti. *Connect. Tissue Res.* 29:191–201.
18. Van Camp, G., P. J. Willems, and R. J. H. Smith. 1997. Nonsyndromic hearing impairment: unparalleled heterogeneity. *Am. J. Hum. Genet.* 60:758–764.
19. McGuirt, W. T., S. D. Prasad, A. J. Griffith, H. P. Kunst, G. E. Green, et al. 1999. Mutations in COL11A2 cause non-syndromic hearing loss (DFNA13). *Nat. Genet.* 23:413–419.
20. Maison, S. F., A. E. Luebke, M. C. Liberman, and J. Zuo. 2002. Efferent protection from acoustic injury is mediated via $\alpha$9 nicotinic acetylcholine receptors on outer hair cells. *J. Neurosci.* 22:10838–10846.
21. Masaki, K., T. F. Weiss, and D. M. Freeman. 2006. Poroelastic bulk properties of the tectorial membrane measured with osmotic stress. *Biophys. J.* 91:2356–2370.
22. Freeman, D. M., K. Masaki, A. R. McAllister, J. L. Wei, and T. F. Weiss. 2003. Static material properties of the tectorial membrane: a summary. *Hear. Res.* 180:11–27.
23. Weiss, T. F., and D. M. Freeman. 1997. Equilibrium behavior of an isotropic polyelectrolyte gel model of the tectorial membrane: the role of fixed charges. *Aud. Neurosci.* 3:351–361.
24. Sigworth, F. J., and K. G. Klemic. 2002. Patch clamp on a chip. *Biophys. J.* 82:3056–3062.
25. Ghaffari, R., A. J. Aranyosi, and D. M. Freeman. 2005. Measuring the electrical properties of the tectorial membrane. *In* Abstracts of the Twenty-Eight Annual Midwinter Research Meeting. Association for Research in Otolaryngology, New Orleans, LA.
26. Horn, B. K. P. 1986. Robot Vision. MIT Press, Cambridge, MA.
27. Horn, B. K. P., and E. J. Weldon, Jr. 1988. Direct methods for recovering motion. *Int. J. Comp. Vis.* 2:51–76.
28. Brown, M. R., M. S. Tomek, L. Van Laer, S. Smith, J. B. Kenyon, et al. 1997. A novel locus for autosomal dominant nonsyndromic hearing loss, DFNA13, maps to chromosome 6p. *Am. J. Hum. Genet.* 61:924–927.
29. Munyer, P. D., and B. A. Schulte. 1994. Immunohistochemical localization of keratan sulfate and chondroitin 4- and 6-sulfate proteoglycans in subregions of the tectorial and basilar membranes. *Hear. Res.* 79:83–93.
30. Hasko, J. A., and G. P. Richardson. 1988. The ultrastructural organization and properties of the mouse tectorial membrane matrix. *Hear. Res.* 35:21–38.
31. Keefe, D. H., F. Zhao, S. T. Neely, M. P. Gorga, and B. R. Vohr. 2003. Ear-canal acoustic admittance and reflectance effects in human neonates. I. Predictions of otoacoustic emission and auditory brainstem responses. *J. Acoust. Soc. Am.* 113:389–406.
32. Masaki, K., D. M. Freeman, G. Richardson, and R. J. H. Smith. 2006. Measuring the material properties of normal and mutant tectorial membranes. *In* Auditory Mechanisms: Processes and Models. A. L. Nuttall, editor. World Scientific, Singapore.
33. Reference deleted in proof.
34. Thalmann, I., G. Thallinger, T.H. Comegys, and R. Thalmann. 1985. Tectorial membrane—a collagen based gel? *In* The 110th Meeting of the Acoustical Society of America. The Acoustical Society of America, Nashville, TN.
35. Shoelson, B., E. K. Dimitriadis, H. Cai, B. Kachar, and R. S. Chadwick. 2004. Evidence and implications of inhomogeneity in tectorial membrane elasticity. *Biophys. J.* 87:2768–2777.
36. Mendler, M., S. G. Eich-Bender, L. Vaughan, K. H. Winterhalter, and P. J. Bruckner. 1989. Cartilage contains mixed fibrils of collagen types II, IX, and XI. *Cell Biol.* 108:191–197.
37. Eikenberry, E. F., M. Mendler, R. Burgin, K. H. Winterhalter, and P. Burckner. 1992. Fibrillar organization in cartilage. *In* Articular Cartilage and Osteoarthritis. K. E. Kuettner, R. Schleyerbach, J. C. Peyron, and V. C. Hascall, editors. Raven Press, New York.
38. Li, Y., D. A. Lacerda, M. L. Warman, D. R. Beier, H. Yoshioka, et al. 1995. A fibrillar collagen gene, Col11a1, is essential for skeletal morphogenesis. *Cell.* 80:430–435.
39. Park, S., and G. A. Ateshian. 2006. Dynamic response of immature bovine articular cartilage in tension and compression, and nonlinear viscoelastic modeling of the tensile response. *ASME J. Biomech. Eng.* 128:623–630.
40. Hayes, W. C., and A. J. Bodine. 1978. Flow-independent viscoelastic properties of articular cartilage matrix. *J. Biomech.* 11:407–419.
41. Bergel, D. H. 1961. The dynamic elastic properties of the arterial wall. *J. Physiol.* 156:458–469.
42. Fung, Y. C. 1981. Biomechanics: Mechanical Properties of Living Tissues. Springer-Verlag, New York, NY.
43. Gueta, R., D. Barlam, R. Z. Shneck, and I. Rousso. 2008. Sound-evoked deflections of outer hair cell stereocilia arise from tectorial membrane anisotropy. *Biophys. J.* 94:4570–4576.
44. Gueta, R., E. Tal, Y. Silberberg, and I. Rousso. 2007. The 3D structure of the tectorial membrane determined by second-harmonic imaging microscopy. *J. Struct. Biol.* 159:103–110.